CrystEngComm

Accepted Manuscript

ROYAL SOCIETY OF CHEMISTRY

www.rsc.org/crystengcomm

CREATED USING THE RSC LaTeX PCCP ARTICLE TEMPLATE – SEE www.rsc.org/electronicfiles FOR DETAILS

ARTICLE TYPE www. rsc.org/xxxxxx | XXXXXXXX

Epitaxial growth of gadolinium and lutetium-based aluminum perovskites thin films for X-rays micro-imaging applications

F. Riva,*[a,c] P-.A. Douissard,[a] T. Martin, [a] F. Carlà, [a] Yu. Zorenko, [b] and C. Dujardin *[c]

Received Xth XXXXXXXXXX 20XX, Accepted Xth XXXXXXXXX 20XX

First published on the web Xth XXXXXXXXXX 200X

DOI: 10.1039/b000000x

Our work is related to the liquid phase epitaxy based development of new scintillating screens for high-resolution X-ray imaging. We successfully grew undoped and Tb, Eu or Ce-doped $GdAlO_3$ as well as $Gd_xLu_{1-x}AlO_3$ single crystalline films on $YAlO_3$ substrates. We studied the crystallization conditions as a function of the melt composition, growth temperature and lattice mismatch between the film and the substrate. The film composition was measured by electron micro probe and the morphology of the film surface was studied by scanning electron microscopy; X-ray diffraction was used to characterize the crystal structure and the mismatch between the film and the substrate. In addition, the light yield of the Eu^{3+} doped films, as well as the obtained spatial resolution show that $Gd_xLu_{1-x}AlO_3$ may advantageously compete with existing thin film scintillators in particular energy ranges.

1 Introduction

Thin single crystal films (SCFs) are used as state of the art scintillating screens for X-rays micro-imaging 2D detectors, particularly at micro and sub-micrometer resolution, where few-micrometer-thick films are required[1–3]. Currently at third-generation synchrotrons, scientists can perform experiments using tender and hard X-rays, opening the door for the study of new techniques and more different samples[4,5]. However, at high energy, the detector is inefficient due to the low absorption of thin scintillators, which becomes the main limitation. As an illustration, 10 μm of gadolinium gallium garnet $Gd_3Ga_5O_{12}$ (GGG), a material currently used as scintillator at the European Synchrontron Radiation Facility (ESRF), absorbs less than 20% of incident X-rays at 20 keV, and becomes almost transparent at 100 keV. Moreover, in the case of tender X-rays the detector spatial resolution is mainly limited by visible light diffraction, while in the case of hard X-rays the spatial resolution is limited by the spread of the deposited energy in the scintillator due to secondary X-rays and electrons.

Our work aims to develop a new generation of scintillating films for 2D detectors, to improve the efficiency of the detector and its spatial resolution, specifically for hard X-ray imaging.

[a] *ESRF - The European Synchrotron , 71 avenue des Martyrs 38000 Grenoble, France; E-mail: federica.riva@esrf.fr*

[b] *Institute of Physics, Kazimierz Wielki University in Bydgoszcz, 2 Powstancow Wielkopolskich Str., 85-090 Bydgoszcz, Poland*

[c] *Institut Lumière Matiére, UMR5306, Université Claude Bernard Lyon1-CNRS, bâtiment Kastler, 10 rue Ada Byron 69622 Villeurbanne Cedex, France. Fax: (33) 472 431 130; Tel: (33) 472 448 336; E-mail: christophe.dujardin@univ-lyon1.fr*

Two main techniques are currently used to produce thin (1-20 μm) scintillating SCFs: growth on a substrate from a super cooled melt solution by liquid phase epitaxy (LPE) and thinning of a bulk crystal by mechano-chemical polishing method[6]. Mechanical polishing presents some advantages: no contaminations from the melt enters in the film and this technique does not require a specific substrate. It presents however some disadvantages. Firstly, the minimum thickness that can be obtained is limited to approximately 20-25 μm for self-standing crystals and 5-10 μm for crystals glued on a substrate. The depth of field of a microscope objective with a numerical aperture higher than 0.6 is less than 1 μm. Consequently, combining a 10 μm thick SCF with high numerical aperture optics will degrade the spatial resolution because of the defocused image. In addition, a 10 μm thick polished scintillator can only be obtained for a small sample area. Secondly, due to the high temperature and to oxygen-free atmosphere of the bulk growth the scintillators obtained from bulk crystals often present anti-site defects and oxygen vacancies, leading to the presence of a slow component in the luminescence (afterglow).

In our work we use the LPE technique, which presents some advantages. Scintillating screens down to 1 μm thickness can be produced and the technology is not limited to small area samples. In addition, for some materials, LPE films present fewer structural defects compared to bulk crystals, due to the lower growth temperature, leading to a reduction of the afterglow: this effect has been reported for example for $Lu_3Al_5O_{12}$ (LuAG) and for some aluminum perovskites[7,8]. Moreover, using the LPE technique, the dopant concentration can be precisely tuned to maximize the conversion efficiency and the

dopant concentration in the film is very homogeneous. LPE also presents some drawbacks. Firstly, some unwanted impurities from the flux used for the LPE growth can enter in the film. Depending on the nature of these impurities, the quality and the scintillation properties of the film can be degraded. Tous et al.[9] as well as Zorenko et al.[10] have studied the effect of different fluxes on garnet SCFs. The films obtained with a BaO-based flux show better conversion efficiency with respect to the films obtained using a PbO-based flux. However, when a BaO-based flux is used, the optical quality and surface morphology are not as good as compared to a PbO-based flux. Secondly, LPE requires the availability of a non luminescent substrate with the same crystalline structure and low lattice mismatch with respect to the film.

Gadolinium-Gallium garnet $Gd_3Ga_5O_{12}$:Eu (GGG) and lutetium orthosilicate Lu_2SiO_5:Tb (LSO) SCFs produced by LPE are currently the state of the art scintillators for high-resolution imaging detectors at the ESRF[1,11,12].

Rare-earth aluminum perovskites are good candidates to improve the efficiency of the scintillators while keeping the same spatial resolution because of the high densities and the high effective Z number. Moreover, they show good luminescence efficiencies when doped by appropriate rare-earth ions[13,14]. In particular, $GdAlO_3$ (GdAP) and $LuAlO_3$ (LuAP) are good scintillator candidates for imaging experiments at relatively high X-ray energies (50-75 keV) due to the position of their absorption K-edges. In table 1, the calculated absorption for SCF perovskites for different energies as well as GGG, LSO and LuAG are reported, highlighting the potential improvement of GAP based film detectors in the energy range of Gd K-edge. In addition, the bulk growth of YAP is well developed and YAP substrates with good crystalline quality are commercially available at a relatively low price. This condition is required if SCFs are to be used as part of X-ray detectors. If comparable light yield is obtained as compared to GGG:Eu^{3+}, increased factor of merit (FOM = absorption $\times$ Light Yield) is expected.

Table 1 Calculated absorption (η) for 10 μm thick at different X-ray energies.

	GGG	LSO	GdAP	GdLuAP	LuAG
η at 15keV	40.5 %	50.9 %	38.4 %	46.0 %	41.0 %
η at 52keV	6.1 %	2.7 %	8.4 %	5.7 %	2.0 %
η at 64keV	3.6 %	7.0 %	5.0 %	6.1 %	5.2 %

Zorenko et al.[7] have investigated the LPE growth of $ReAlO_3$ (Re = Y, Lu, Tb) on YAP substrates; in the frame of X-ray imaging applications, we have presented results about LuAP SCFs on YAP substrates[15]. To the best of our knowledge, optically good GdAP can not be grown using bulk techniques (i.e. Czochralsky or Bridgman). However, the possibility of growing GdAP crystals by the flux method has been reported for an other purpose than scintillators[16,17]. The addition of lutetium may play a role in stabilizing the crystal during the growth as well as tuning the absorption efficiency exploiting the K-edges of Lu and Gd. Unlike GdAP, GdLuAP ($Gd_{1-x}Lu_xAlO_3$) has been successfully grown using the Czochralsky method[18,19]. In the case of LPE the lattice mismatch between the film and the substrate plays a critical role in the crystalline structure and in the luminescence properties of the film. For instance, Kucera at al.[20] report this effect for lutetium and yttrium aluminum garnets, while previously Stringfellow[21] has shown it in the case of $Ga_xIn_{1-x}P$ on GaAs substrates.

We developed the LPE growth process for GdAP and GdLuAP on YAP substrates using a PbO-B_2O_3 flux. The growth conditions and the crystal structure are presented in this paper, as well as scintillation and X-ray imaging properties. A careful optimization of the growth parameters was performed to get SCFs with optimal optical quality and light yield. We grew several series of GdAP and GdLuAP films, both undopped and Eu, Tb or Ce doped. Particularly, we adjusted the lattice parameters of the film by modifying the Gd/Lu ratio: moving from a GdAP to a GdLuAP films, we obtained the best optical quality of the screen. Thanks to those efforts, we tested GdLuAP SCFs for X-ray imaging and demonstrate that they are a good competitor as compared to existing SCFs.

2 Experimental

2.1 LPE growth of GdAP and GdLuAP SCFs

GdAP and GdLuAP epitaxial single crystalline films were grown using LPE on YAP substrates of crystallographic orientation (001), (100) and (011) (defined in the Pbnm space group), produced by the Czochralsky method by MaTeck GmbH, Neyco and Scientific Materials Corp. Several series of samples of undoped and Ce, Tb or Eu doped films were grown from a PbO-B_2O_3 flux using Gd_2O_3, Lu_2O_3, Al_2O_3, Eu_2O_3, Tb_4O_7 and Ce_2O_3 5N pure starting powders. The melt was contained in a Pt crucible and the growth was performed by the isothermal vertical dipping method[22]. The sample was attached to a Pt sample holder, which rotated during the growth at a speed of 70 rpm, with alternate direction of the rotation every 5 s. The thicknesses of the films was determined by their weight gain and ranged from 0.3 to 30 μm. The growth was performed at temperatures between 980 and 1080°C resulting in growth rates of 0.05 to 2.34 μm/min.

2.2 Characterization of the films

The composition of the film was analyzed using a Castaing Cameca SX50 electron micro probe (EMP) equipped with

tungsten cathode and 4 vertical spectrometers. The acceleration voltage of the cathode was 22 kV.
The surface morphology was investigated using a LEO 1530 scanning electron microscope (SEM).
The crystallographic structure of the GdAP or GdLuAP films and the lattice mismatch with the YAP substrate have been evaluated using X-ray diffraction (XRD) on a vertical reflectometer at the BM05 beamline at the ESRF (Grenoble). The X-ray energy was set to 15 keV using a double crystal Si(111) monochromator. The diffraction spectra were recorded using a silicon diode. The in-plane diffraction experiments were carried out using a six circle z-axis diffractometer installed at the ID03 beamline of the ESRF (Grenoble)[23]. The sample was kept in an Argon flow during the experiment in order to prevent damages induced by oxygen and ozone. In order to be able to penetrate the film and identify the cystallographic orientation of the substrate the energy of the incident beam was 24 keV. The data were acquired using a Maxipix detector, data reduction and analysis have been performed using BINoculars[24].
To evaluate the light yield (LY), the scintillator was irradiated by 8 keV X-rays and the signal was recorded by a PCO Sensicam camera, combined with 2X optics. The signal intensity was corrected by the calculated absorption of the X-rays in the scintillator and by the sensors quantum efficiency and compared to the signal obtained with a YAG:Ce bulk sample chosen as reference (produced by Crytur). The photoluminescence spectra were measured at room temperature (RT) using a Horiba/Jobin-Yvon Fluorolog-3 spectrofluorimeter with a 450 W xenon lamp and a Hamamatsu R928P photomultiplier. The photoluminescence excitation (PLE) spectra were corrected for the xenon lamp emission spectrum.

3 Results and discussion

3.1 LPE growth of GdAP and GdLuAP

Several series of GdAP and GdLuAP thin films have been grown by LPE in PbO-B_2O_3 flux, on YAP substrates oriented (100), (001) and (110).

Figure 1 shows the concentration triangle for the pseudo-ternary system of the melt. The system composed by Pb, B, Al, Gd and Lu is reduced to a pseudo-ternary system on the three axes of which the relative atomic concentration of Pb+B (flux), Al and Gd+Lu is reported. The round marks represent the conditions in which the growth of an aluminum perovskite film covering the overall surface of the substrate was achieved, regardless of the quality of the film (figure 2a-2b). The color represents the different ratio R_{Lu}. We found that the melt was stable when the atomic ratio $\frac{Pb}{B}$ is kept between 5 and 6, meaning that the growth speed is linear with the temperature (and repeatable over different samples) and no spontaneous crystal-

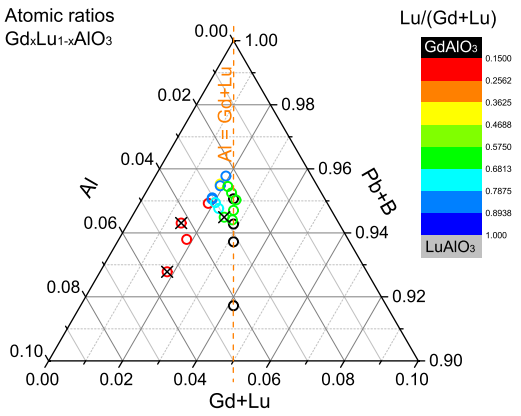

Fig. 1 Concentration triangle of the pseudo-ternary system $Gd+Lu$, Al, $Pb+B$ studied for the LPE growth of $Gd_xLu_{1-x}AlO_3$ on $YAlO_3$. The color of the round marks indicated the $\frac{Lu}{Gd+Lu}$ ratio. The black crosses indicate when the crystallization of islands is preferred to the film growth.

lization at the surface of the melt or on the stirrer is observed. For the optimized composition (R_{Lu} = 0.55-0.58) Pb/B = 5.20-5.30, the Pb content as contaminant in the as grown films was measured using the microprobe technique and it ranges between 0.008% and 0.01%. The microprobe data were taken from 10 different points on every sample. Because we are at the limit of the microprobe sensitivity, the observed standard deviation over these 10 points is in the order of the measured values. The black crosses indicate the melt concentration where the crystallization of islands (with a different composition with respect to the film) was observed (Figure 2e-2f). Along the vertical orange dashed line the atomic concentration of Al and Gd+Lu in the melt agreed with the stoichiometry of the perovskite phase (i.e. R_{Al} = 1). The growth parameters and the Al, Gd and Lu relative concentration in the melt are reported in table 2. When islands were crystallized together with the film, the thickness and the growth rate is not reported, due to the lack of precise evaluation by the weighing method.

The best optical and structural morphology was obtained for R_{Lu} between 0.55 and 0.58. In figure 3, the growth speed for different substrate orientations is reported as function of the temperature. The samples are grown from the same melt where R_{Lu} was fixed at 0.55. Small variations from the expected linear dependence in the growth speed can be observed: these variations are expected, considering the gradual change of the melt composition, due to its evaporation and due to the Eu_2O_3 additions performed to optimize the dopant concentration.

The films composition has been evaluated by EMP. In figure 3, the R_{Lu}^{film} (in the film) with respect to R_{Lu}^{melt} (in the melt)

Table 2 Atomic ratios between Gd, Lu and Al in the melt ($R_{Lu} = \frac{Lu}{Gd+Lu}$ and $R_{Al} = \frac{Al}{Gd+Lu}$, obtained structure (Str.) (f = film, i = islands), thickness (Th.) and growth rate (G.R.) for LPE growth of $Gd_xLu_{1-x}AlO_3$ on YAP. When islands were crystallized, the thickness and the growth rate is not reported due to the impossibility of a precise evaluation by weighing method.

R_{Lu}	R_{Al}	Str.	Th.[μm]	T[°C]	G.R.[$\frac{\mu m}{min}$]
0	1	f	4.2-27.8	1030±40	0.4-2.78
0.2	1.73-2.38	f	0.4-5.3	1050±10	0.05-0.49
0.2	2.97	f+i	-	1060±10	-
0.4	1.38	f	0.3-21.0	1010±10	0.03-1.38
0.55-0.58	1-1.05	f	1.0-23.0	1015±10	0.15-2.3
0.65	0.95-1.15	f+i	-	1010±20	-
0.85	1.21-1.61	f+i	-	1010±15	-

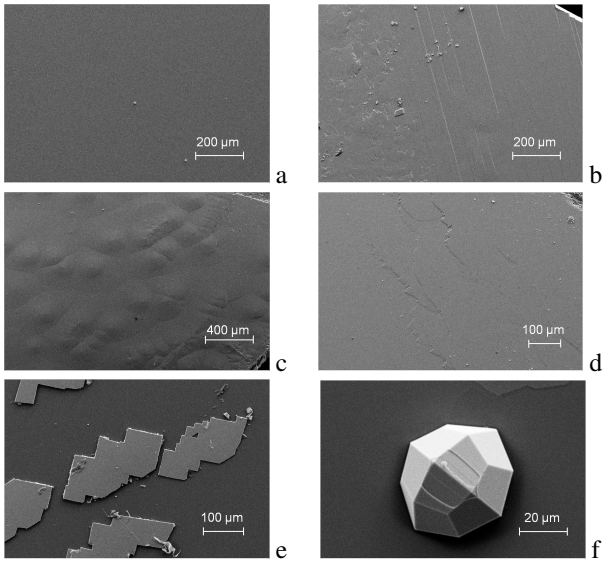

Fig. 2 SEM images of different surface morphologies obtained for different conditions. (a),(b): $Gd_{.45}Lu_{.55}AlO_3$ film (low lattice mismatch with the substrate) for substrates from different suppliers. (c),(d): $Gd_{.10}Lu_{.90}AlO_3$ film (high lattice mismatch with the substrate) for substrates from different suppliers. (e),(f): Island growth in the case of excess Al concentration in the melt.

is reported for different samples; to highlight deviations, the line corresponds to the case R_{Lu}^{melt} equal to R_{Lu}^{film}. A dependence of the R_{Lu}^{film} ratio on the substrate orientation has been observed. For example, when R_{Lu}^{melt} is equal to 0.55, the Lu concentration in the film is considerably lower for the (001)-oriented samples than for (100) and (011) oriented samples, respectively. We assign this effect to the growth temperature: in order to have a growth rate of 0.3 $\mu m/min$, the required temperature for the (001)-oriented substrates is ≈ 12°C lower than for the (011)-oriented samples. This difference may also

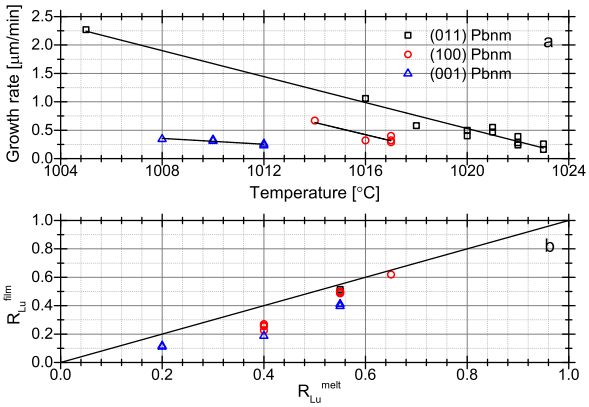

Fig. 3 (a) Growth speed of the film as function of the temperature, for R_{Lu}^{m} =0.55. (b) R_{Lu} in the film with respect to R_{Lu} ratio in the melt, measured by EMP, for different substrate orientations. The reference line refers to the case in which the stoichiometry of the obtained film is the same as the elements ratio in the melt.

have effects in the scintillation properties (see section "scintillation and imaging properties"). In addition, for all the studied samples, R_{Lu}^{film} is always lower than R_{Lu}^{melt}. This effect need to be taken into account in order to control the lattice mismatch and therefore, the film optical quality and crystal morphology.

3.2 Film characterization: crystalline structure and surface morphology

By varying the Lu percentage in the melt composition, and therefore in the film, different surface morphologies have been observed (figure 2). Depending on the substrate orientation, an optimal concentration of Lu and Gd in the melt leads to a homogeneous film surface (figure 2a), while for a different melt composition the film surface is wavy (figure 2c) and the optical quality of the film is not good enough for imaging. The best results were obtained for R_{Lu} between 0.5 and 0.6.
The optical quality of the film, which is strictly connected to the crystalline quality and to the surface morphology, depends on the lattice mismatch between the substrate and the film. In table 3, the lattice parameter values for GdAP[25], LuAP[26] and YAP[27] single crystals are reported: the calculated mismatch between GdAP (or LuAP) and YAP is different in the three crystallographic directions due to the orthorhombic structure. A significant mismatch reduction can be achieved for $Gd_xLu_{1-x}AlO_3$ for $x \approx 0.5$.

Figure 4 shows the omega-2theta scans at 15 keV around the (400) symmetric reflection for the (100) oriented samples (a) and around the (002) symmetric reflection for the (001) oriented samples (b). The ratio between the diffracted intensities of the substrate and the film is not constant among the

Table 3 Lattice parameters of GdAP, LuAP and YAP single crystals from literature[25–27] and calculate lattice mismatch. Lattice parameters in Å.

	a	b	c	cell vol.
GdAP[25]	5.2537	5.3049	7.4485	207.5923
LuAP[26]	5.0967	5.3294	7.2931	198.0957
YAP[27]	5.1803	5.3295	7.3706	203.4895
GdAP-YAP	+1.417 %	-0.462 %	+1.057 %	+2.016 %
LuAP-YAP	-1.614 %	-0.002 %	-1.051 %	-2.650 %
$Gd_{.5}Lu_{.5}AP - YAP$	-0.098 %	-0.232 %	0.003 %	-0.317 %

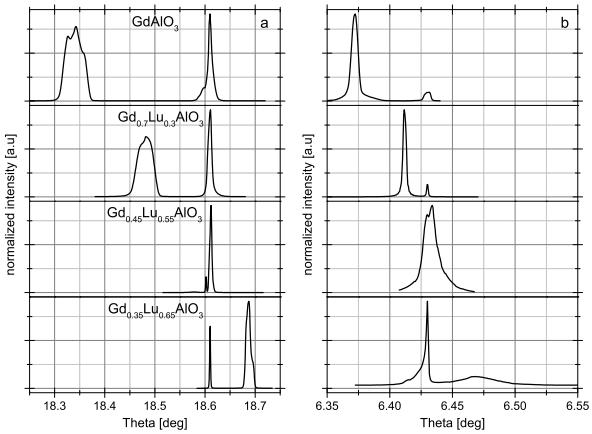

Fig. 4 Omega-2theta scans for different films of $Gd_xLu_{1-x}AlO_3$. (a): scans around the 400 reflection, YAP substrate (100)-oriented, substrate peak at 18.56°. (b): scans around the 002 reflection, YAP substrate (001)-oriented, substrate peak at 6.43°. The approximate composition of the film is reported in the legend, 15 keV X-ray energy.

different samples, due to differences in film thickness, composition and crystal structure. The lattice mismatch has been evaluated from the distance between the GdLuAP diffraction peak and the YAP diffraction peak: the measured value of the lattice mismatch for different samples is reported in figure 5, as a function of the R_{Lu}^{film}. Since the composition was not measured for all the samples, we approximate the composition of the films grown at the same melt concentration to the composition of the measured samples. However, a slight difference in the R_{Lu} ratio between different samples can be observed, mainly due to differences in temperature and growth rate. This effect has to be taken into account as source of error for the results reported in this plot.

As expected, we observe a reduction of the distance between the two peaks going towards $Gd_{0.45}Lu_{0.55}AlO_3$. However, the minimum mismatch in the two directions does not occur at the same film composition.

We can observe in figure 4 the broad and asymmetric peaks related to the films. Such a peak shape (asymmetric, broader) is typical for quasi-heteroepitaxial growth with relatively large lattice mismatch (above 1%). It indicates a worse structural quality of films due to some deviations in their content, plane orientation, and formation of the film/substrate transition layer. Thus, the SCF is still single crystalline but possesses a worse structural quality than in the homo-epitaxy case (figure 4, left column, graphs for $Lu_{0.55}Gd_{0.55}AO_3$:Eu sample). In the right column for this R_{Lu} the peaks from the substrate and the film strongly overlap and resemble as a broader peak. Together with the reduction of the lattice mismatch, we observe then a reduction of the width of the diffraction peak of the film, indicating an improvement of the film's crystal structure. This effect is confirmed by the evaluation of the rocking curve (RC): in figure 6-top, the RC for the substrate and the film is reported for two different samples, grown on the same kind of substrate and at the same conditions, except for the different R_{Lu} ratios. In the case of $Gd_{0.9}Lu_{0.1}AlO_3$, R_{Lu} is equal to 0.2 in the melt, $\Delta c \approx +0.8\%$ along the (001) direction and the observed peak for the film is much larger than the substrate, indicating that the crystallinity is deteriorated with respect to the one of the substrate. On the contrary, the RC of $Gd_{0.45}Lu_{0.55}AlO_3$, R_{Lu} is equal 0.55 ($\Delta c \approx +0.25\%$) and the diffraction peak width is similar to the one of the substrate, indicating a similar crystallinity. To separate the potential contribution of the substrate and the film X-ray diffraction response, out of plane diffraction experiments are presented in figure 6-bottom. Since lower incidence angles favor the film response, the film diffraction peak originating from the film can be clearly identified and demonstrates that the film is a single crystal and is oriented as the substrate.

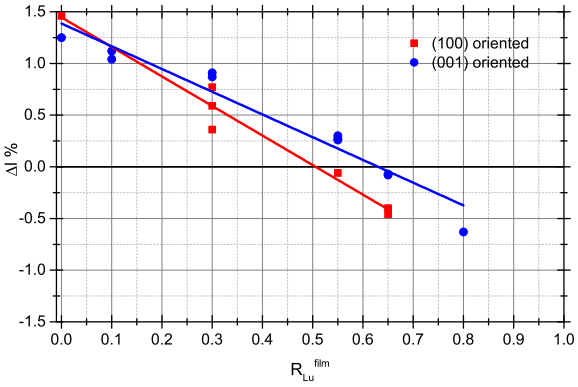

Fig. 5 Lattice parameter mismatch between the YAP substrate and the $Gd_xLu_{1-x}AlO_3$ film ($\Delta l = \frac{l_{film} - l_{subtrate}}{l_{substrate}}$), evaluated along the direction perpendicular to the surface by XRD; the composition was measured by EMP.

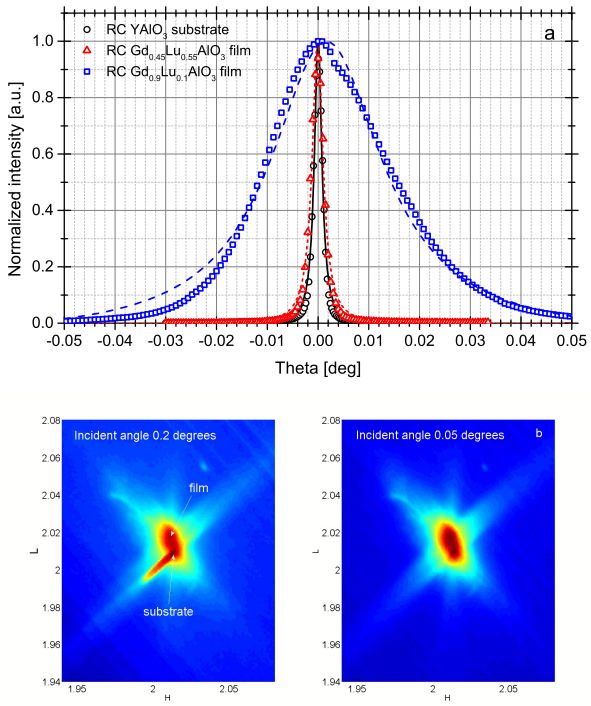

Fig. 6 -a- Rocking curves around the (002) reflection for GdLuAP films and YAP substrates (black circles),(001)-oriented. For comparison of the Full Width Half Max, the spectra have been shifted to set the maximum of the peak at 0°. Red triangles correspond to the case of the low lattice mismatch ($Gd_{0.45}Lu_{0.55}AlO_3$) and the blue squares to the high lattice mismatch case ($Gd_{0.9}Lu_{0.1}AlO_3$). -b-: Reciprocal space map around the (212) reflection for $Gd_{0.45}Lu_{0.55}AlO_3$ film on YAP substrate (001)-oriented, recorded at 24 keV. To enhance the substrate and the film contribution the maps have been recorded at incident angle 0.2° (left) and at incident angle 0.05° (right).

3.3 Scintillation and imaging properties

The perovskite SCFs can be doped with various rare earth ions ensuring the scintillation properties. The dopant concentrations of the Eu^{3+} doped samples are presented in figure 8-a-, while the Tb^{3+} and Ce^{3+} are respectively 6.3% and 0.49%. In figure 7 the emission spectra under UV excitation of GdAP:Tb^{3+}, GdAP:Ce^{3+} and GdLuAP:Eu^{3+} are reported. Eu^{3+} and Tb^{3+} exhibit the expected emission lines from of the f-f recombination, respectively in the red and green ranges. Note that no divalent europium emission is observed. The Ce^{3+} doped sample shows a broad UV band due to the d-f radiative recombination. The maximum wavelength peaking at 360 nm is typical for the cerium emission in perovskite phases. As shown in XRD, no residual garnet phase can be observed. If the various activators can enter in the films, our final aim is to obtain the best light yield, combined with an appropriate emission wavelength for used camera and offering a good optical quality for imaging under microscopy. So far, we focused on the optimization of Eu^{3+} doped GdLuAP SCFs, with $R_{Lu} \approx 0.55$. As described above, this composition shows the smallest lattice mismatch with YAP substrates. This composition leads thus to the best optical quality SCFs which is crucial for imaging and to proper scintillation yield evaluation.

Using a standard experimental set-up including a pulsed excitation source operating at 404 nm, we have measured the fluorescence decay time of GdLuAP:Eu^{3+} at 614 nm emission wavelength and found a value of 1.49 ms. This means that Eu doped perovskite SCF are suitable for imaging experiments at acquisition frame rate lower than 500 Hz.

In figure 8-b- the LY of different GdLuAP SCFs is reported as a function of the percentage of the YAG:Ce bulk LY. Note that the measurement has been corrected by the absorption. The density being in the same order of magnitude, we also expect having similar penetration depth of the X-rays in the samples enabling to consider similar light collection efficiency from sample to sample. On the (011)-oriented substrates, the optimized light yield is about 90 % of the YAG:Ce bulk scintillator used as reference. The LY of the GGG:Eu^{3+} SCFs is around 70 % while the currently used LSO:Tb SCF shows a scintillation yield of 100 %. In terms of efficiency, the GdLuAP:Eu SCFs can therefore compete with the existing SCFs, especially in the energy range 52-63 keV, where the absorption of the Lu-based materials is lower than the Gd-based ones: the factor of merit is higher than the other available SCFs (5.13 versus 4.27 for GGG and 2.7 for LSO at 52 keV). Surprisingly, we observed that the scintillation yield depends strongly on the substrate orientation: it is only 20 % for (001) oriented and 40-50 % for the (100) oriented ones. The reason for this difference is not yet clear and requires more detailed investigations. So far, we can exclude that it could be due to a different segregation coefficient of Eu and therefore, to a different Eu

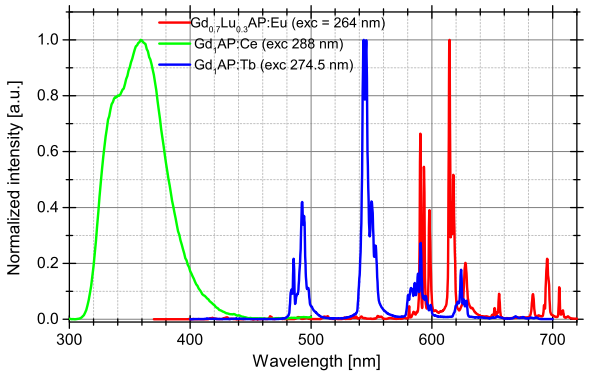

Fig. 7 Emission spectra of GdAP:Ce, GdAP:Tb and GdAP:Eu SCFs under UV excitation.

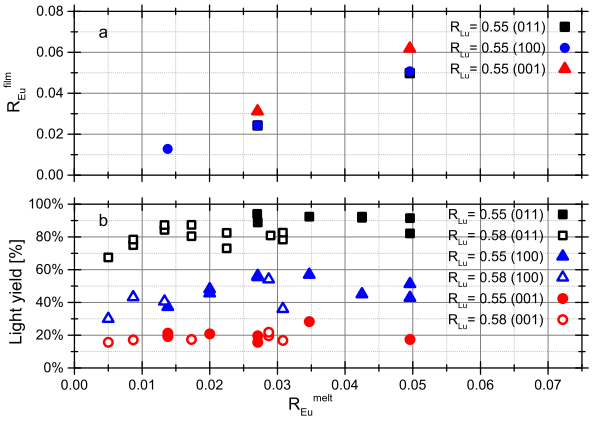

Fig. 8 -a- Eu concentration in the film as a function of the Eu concentration in the melt for Gd $_{0.45}Lu_{0.55}AlO_3Eu^{3+}$. -b- Light yield of Gd $_xLu_{1-x}AlO_3Eu^{3+}$ for different YAP substrate orientations. The emitted light is recorded using a high-resolution setup and the measurement is corrected for absorption and detector quantum efficiency.

concentration in the film. The Eu concentration in the films was measured by EMP and the obtained values are similar for samples of different orientations grown at the same melt concentration 8-a. Moreover, the Eu concentration in the melt was varied from R_{Eu}^{film} 0.5 % to 5 %: in this range, no significant variation of the scintillation yield was observed. Therefore, we expect that this difference is mainly due to the different strain and defects that could lead to a different efficiency of the energy transfer between the perovskite crystal and the Eu atoms. In particular, we expect a significant difference in the segregation coefficients of Pb^{2+} from the flux due to different growth temperatures and a different substrate-film mismatch for the different orientations: Pb^{2+} is in fact a quencher of the radiative emission and can therefore have a negative influence on the scintillation properties. If that is the case, at a different R_{Lu}^{film} ratio the LY could show a different behavior with respect to the substrate orientation.

The optimized GdLuAP:Eu^{3+} SCFs on YAP substrates were polished down to 120 μm from the substrate side and the imaging properties were tested at the beamline BM05 at the ESRF. In figure 9 top, we show the images of various patterns and deduce the contrast as a function of the spatial frequency for the bulk YAG, GGG:Eu, the current state of the art, and the new optimized scintillating screen made of GdLuAP:Eu. We clearly show that the combination of the good light yield and optical quality give rise to a contrast improvement in the small spatial frequencies by a factor of 10% . To demonstrate the imaging capabilities, we also present in figure 9 (bottom) the X-ray radiography of a fly at 12 keV. As comparison, the same image was taken with a 11 μm GGG:Eu SCFs. The two images show comparable image quality and demonstrate that the GdLuAP:Eu screens can compete with the GGG:Eu films. Moreover, the higher light yield of GdLuAP:Eu allows shorter exposures, which is crucial when tomography imaging and time-resolved applications are performed.

4 Conclusion

We demonstrated the feasibility of the crystallization of GdAP and GdLuAP SCFs on YAP substrates using LPE. The best fraction of Lu that render the smallest lattice mismatch from the film and the YAP substrate is given by $R_{Lu} \approx 0.55$. For this ratio, we optimized the melt composition and growth parameters that are required to crystallize the perovskite phase using $PbO - B_2O_3$ flux while respecting the optical and structural quality of the film. We optimized the GdLuAP:Eu^{3+} doped SCF for high resolution imaging applications. Compared to the GGG:Eu currently used at synchrotrons for high resolution imaging, contrast performances are better. GdLuAP:Eu^{3+} can therefore complete with LSO and GGG the high performance SCFs family. X-ray imaging is performed at various energies in synchrotron facilities and X-ray absorption varies a lot around the element absorption edges. This compound exhibits a better absorption in the energy range 52-63keV. It is therefore a functional SCF material for X-ray imaging detectors with frame rate below 500 Hz. For faster imaging acquisition, the faster scintillator GdLuAP:Ce^{3+} can be a good candidate for ultra-fast imaging (decay time $\approx$ 50 ns), but due to the emission peaking at 360 nm, it requires a UV sensitive optics and camera.

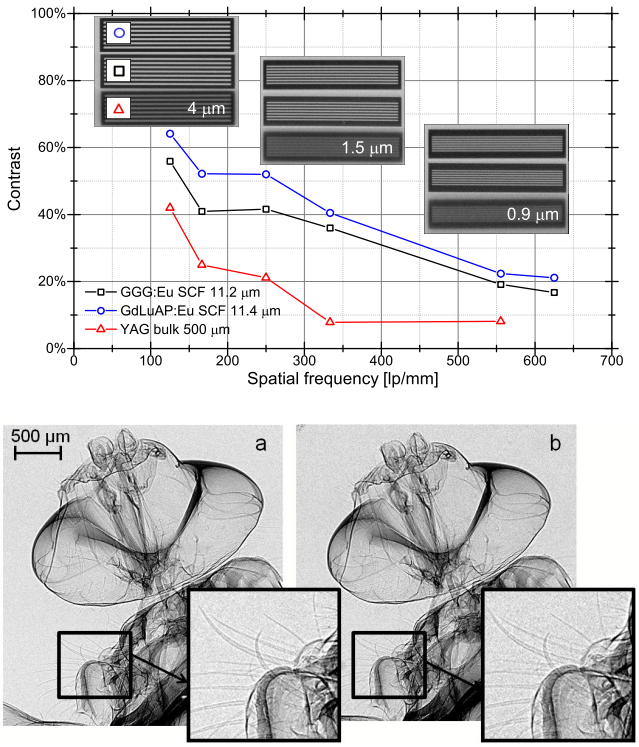

Fig. 9 Top: Images of a tungsten pattern and deduced contrast as a function of the spatial frequency, recorded using a PCO2000 camera coupled with a 20X objective, NA = 0.4. Bottom: Image of a fly with GdLuAP:Eu 11.4 μm scintillator (a) and with a 11.2 μm GGG:Eu scintillator (b), recorded using a PCO2000 camera coupled with a 2X microscope objective, NA = 0.08.

5 Aknowledgement

Part of this work has been performed in the frame of the Polish NCN 2012/07/B/ST5/02376 project. The authors thank E.Ziegler and the BM05 staff, as well I.Snigireva for the SEM images at the microimaging laboratory at ESRF.

References

1 T. Martin and A. Koch, *J. Synchrotron Rad.*, 2006, **13**, 180–194.
2 A. Koch, C. Raven, P. Spanne and A. Snigirev, *JOSA A*, 1998, **15**, 1940–1951.
3 A. Pereira, T. Martin, M. Levinta and C. Dujardin, *J. Mater. Chem. C*, 2015, **3**, 4954–4959.
4 A. Snigirev, I. Snigireva, V. Kohn, S. Kuznetsov and I. Schelokov, *Rev. Sci. Instrum.*, 1995, **66**, 5486–5492.
5 P. Tafforeau, R. Boistel, E. Boller, A. Bravin, M. Brunet, Y. Chaimanee, P. Cloetens, M. Feist, J. Hoszowska and J.-J. Jaeger, *Appl. Phys. A*, 2006, **83**, 195–202.
6 M. Nikl, J. Tous, J. Mares, P. Prusa, E. Mihokova, K. Blazek, A. Vedda, Y. Zorenko, V. Gorbenko and V. Babin, SPIE Defense, Security, and Sensing, 2009, pp. 731008–731008.
7 Y. V. Zorenko and V. Gorbenko, *Phys. Solid State*, 2009, **51**, 1800–1808.
8 M. Kučera, K. Nitsch, M. Nikl, M. Hanuš and S. Daniš, *J. Cryst. Growth*, 2010, **312**, 1538–1545.
9 J. Tous, K. Blazek, M. Kucera, M. Nikl and J. A. Mares, *Radiat. Meas.*, 2012, **47**, 311–314.
10 Y. Zorenko, J. Mares, P. Prusa, M. Nikl, V. Gorbenko, V. Savchyn, R. Kucerkova and K. Nejezchleb, *Radiat. Meas.*, 2010, **45**, 389–391.
11 P.-A. Douissard, A. Cecilia, T. Martin, V. Chevalier, M. Couchaud, T. Baumbach, K. Dupré, M. Kühbacher and A. Rack, *J. Synchrotron Rad.*, 2010, **17**, 571–583.
12 T. Martin, P.-A. Douissard, M. Couchaud, A. Cecilia, T. Baumbach, K. Dupre and A. Rack, *IEEE Trans. Nucl. Sci.*, 2009, **56**, 1412–1418.
13 C. Shilpa, A. Kadgathur Jayaram, N. Dhananjaya, H. Nagabhushana, S. Prashantha, D. Sunitha, S. Sharma, C. Shivakumara and B. Nagabhushana, *Spectroc. Acta A*, 2014, **133**, 550558.
14 J. Y. Park, H. C. Jung, G. S. R. Raju, B. K. Moon, J. H. Jeong, S.-M. Son and J. H. Kim, *Mater. Res. Bull.*, 2010, **45**, 572 – 575.
15 P.-A. Douissard, T. Martin, F. Riva, E. Mathieu, Y. Zorenko, V. Savchyn, T. Zorenko and A. Fedorov, *IEEE Trans. Nucl. Sci.*, 2014, **61**, 433–438.
16 J. Andreeta and B. Jovanic, *Materials Research*, 2000, **3**, 45–49.
17 R. Mazelsky, W. Kramer and R. Hopkins, *J. Cryst. Growth*, 1968, **2**, 209–214.
18 J. A. Mareš, M. Nikl, P. Malỳ, K. Bartoš, K. Nejezchleb, K. Blazek, F. De Notaristefani, C. D'Ambrosio, D. Puertolas and E. Rosso, *Opt. Mater.*, 2002, **19**, 117–122.
19 J. Chval, D. Clement, J. Giba, J. Hybler, J.-F. Loude, J. Mares, E. Mihokova, C. Morel, K. Nejezchleb and M. Nikl, *Nucl. Instr. Meth. Phys. Res. Section A*, 2000, **443**, 331–341.
20 M. Kučera, K. Nitsch, M. Nikl and M. Hanuš, *Radiat. Meas.*, 2010, **45**, 449–452.
21 G. Stringfellow, *Journal of Applied Physics*, 1972, **43**, 3455–3460.
22 J. Robertson, M. Van Tol and J. Heynen, *Philips J. Res*, 1980, **35**, 354–371.
23 O. Balmes, R. van Rijn, D. Wermeille, A. Resta, L. Petit, H. Isern, T. Dufrane and R. Felici, *Catal. Today*, 2009, **145**, 220–226.
24 S. Roobol, W. Underwater, J. Drnec, R. Felici and J. Frenken, *J. Appl. Crystallogr.*, **48**, year.
25 N. Ross, J. Zhao and R. Angel, *J. Solid State Chem.*, 2004, **177**, 3768–3775.

26 L. Vasylechko, A. Senyshyn and D. Trots, *Hasylab Annual Report*, 2007.
27 N. Ross, J. Zhao and R. Angel, *J. Solid State Chem.*, 2004, **177**, 1276–1284.